NUMERICAL ASSESSMENT OF REVERSE-FLOW MUFFLERS USING A SIMULATED ANNEALING METHOD

Min-Chie Chiu
Department of Automatic Control Engineering, Chungchou Institute of Technology, Yuanlin, Changhua 51003, R.O.C.
E-mail: minchie.chiu@msa.hinet.net

Received December 2008, Accepted March 2010
No. 08-CSME-45, E.I.C. Accession 3117

ABSTRACT

Because of the necessity of maintenance and operation in industries in which the equipment layout is occasionally tight, the space for a muffler is constrained. An interest in maximizing the acoustical performance of mufflers within a limited space is of paramount importance. As mufflers hybridized with reverse-flow ducts may visibly increase acoustical performance, the main purpose of this paper is to numerically analyze and maximize their acoustical performance within a limited space. In this paper, a four-pole system matrix for evaluating the acoustic performance —sound transmission loss (*STL*)— is derived by using a decoupled numerical method. Moreover, simulated annealing (*SA*), a robust scheme used to search for the global optimum by imitating the metal annealing process, has been used during the optimization process. Before dealing with a broadband noise, the *STL*'s maximization with respect to a one-tone noise (300 Hz) is introduced for a reliability check on the *SA* method. Moreover, an accuracy check of the mathematical model is performed. Results reveal that the *STL* of a muffler with reverse-flow perforated ducts can be maximized at the desired frequency for pure tone elimination; moreover, the noise reduction for a broadband noise can reach 97.5 dB. Consequently, the approach used for the optimal design of the mufflers is simple and effective.

MÉTHODE DU RECUIT SIMULÉ POUR L'ÉVALUATION NUMÉRIQUE DE L'ÉCOULEMENT INVERSÉ D'UN SILENCIEUX

RÉSUMÉ

Dans l'industrie où la configuration de l'espace pour l'appareillage est parfois limitée, et à cause de la nécessité de faire de la maintenance, ainsi que pour l'opération de l'appareillage, l'espace pour un silencieux est restreint. L'intérêt de maximiser la performance acoustique des silencieux à l'intérieur d'un espace limité est d'une importance capitale. Étant donné que des silencieux hybrides à conduits à écoulement inversé peuvent assurément augmenter la performance acoustique, le but principal de l'article est l'analyse numérique et la maximisation de leur performance acoustique dans un espace limité. Dans notre recherche, un système matricielle à quatre pôles pour l'évaluation de la performance acoustique—perte de transmission sonore (STL) — est dérivé en utilisant une méthode à commande numérique découplé. De plus, la méthode du recuit simulé (SA), un schéma robuste utilisé pour la recherche d'un optimum global en imitant le procédé technique du recuit simulé en métallurgie, a été utilisée durant le processus d'optimisation. Avant de s'intéresser au bruit à large bande, la maximisation de la perte de transmission sonore, pour un bruit d'un ton pur (300 Hz) est introduit pour vérifier la fiabilité de la méthode du recuit simulé (SA). En outre, une vérification de l'exactitude du modèle mathématique est exécutée. Les résultats démontrent que la perte de transmission sonore d'un silencieux avec écoulement inversé et conduits perforés peuvent être maximisés à la fréquence désirée pour l'élimination de bruit d'un ton pur; de plus la réduction du bruit pour un bruit à large bande peut atteindre 97.5 dB. Par conséquent, l'approche utilisée pour le design optimal du silencieux est simple et efficace.

NOMENCLATURE

C_o:	sound speed (m s^{-1})
c_1, c_2:	coefficients
dh_i:	the diameter of a perforated hole on the i-th inner tube (m)
D:	diameter of the tubes (m)
f:	cyclic frequency (Hz)
$Iter$:	maximum iteration
j:	imaginary unit
k:	wave number ($=\frac{\omega}{c_o}$)
kk:	cooling rate in SA
kf_1, kf_2, kf_3, kf_4, kf_5, kf_6:	coefficients in function $\Gamma\Gamma_i = kf_i e^{\lambda\lambda_i x}$
L_1,L_2:	lengths of inlet/outlet straight ducts (m)
L_o:	total length of the muffler (m)
M:	mean flow Mach number
OBJ_i:	objective function (dB)
p:	acoustic pressure (Pa)
$\bar{p}_i$:	acoustic pressure at the i-th node (Pa)
$pb(T)$:	transition probability
Q:	volume flow rate of venting gas (m^3 s^{-1})
S_i:	section area at the i-th node(m^2)
STL:	sound transmission loss (dB)
$SWLO$:	unsilenced sound power level inside the muffler's inlet (dB)
SWL_T:	overall sound power level inside the muffler's output (dB)
t_i:	the thickness of the ith inner perforated tube (m)
$TS1_{ij}$, $TS3_{ij}$:	components of four-pole transfer matrices for an acoustical mechanism with straight ducts
$TPRF2_{ij}$:	components of a four-pole transfer matrix for an acoustical mechanism with reverse-flow perforated ducts
T^*_{ij}:	components of a four-pole transfer system matrix
u:	acoustic particle velocity (m s^{-1})
$\bar{u}_i$:	acoustic particle velocity at the i-th node (m s^{-1})
$u_{i,j}$:	acoustical particle velocity passing through a perforated hole from the ith node to the jth node (m s^{-1})
V_i:	mean flow velocity at the *ith* node (m s^{-1})
ρ_o:	air density (kg m^{-3})
ρ_i:	acoustical density at the ith node
ξ_i:	specific acoustical impedance of the ith inner perforated tube
η_i:	the porosity of the ith inner perforated tube.
λ_i:	ith eigen value of $[\Lambda\Lambda]_{6x6}$
$[\Pi\Pi]_{6x6}$:	the model matrix formed by an eigen vector $\Pi\Pi_{6x1}$ of $[\Lambda\Lambda]_{6x6}$

1. INTRODUCTION

Research on mufflers was started by Davis *et al.* in 1954 [1]. To overcome the exhaust noise of a venting system, the assessment of new perforated-element mufflers was started by Sullivan and Crocker in 1978 [2]. Based on the coupled equations derived by Sullivan and Crocker in 1978 [2], a series of theory and numerical techniques in decoupling the acoustical problems have been proposed [3–7]; however, the restrictions of non-flow and instability problems in the solution still existed; fortunately, Munjal [8] and Peat [9] promulgated the generalized decoupling and numerical decoupling methods in 1987 and 1988 which overcome the drawbacks in the previous

studies. To increase a muffler's acoustical performance, the assessment of a new acoustical element — a reverse-flow mechanism with double internal perforated tubes — was proposed and investigated by Munjal *et al.* in 1987 [8]. Due to the necessity of operation and maintenance within an enclosed machine room, a space-constrained problem within a noise abatement facility occurs; therefore, there is a growing need to optimize the acoustical performance within a fixed space. Yet, the need to investigate the optimal muffler design under space constraints is rarely addressed. In previous papers, the shape optimizations of simple-expansion mufflers were discussed [10–13]. To greatly enlarge the acoustical performance within a fixed space, the acoustical mechanism of the above mufflers hybridized with reverse-flow perforated tubes using a novel scheme of simulated annealing (*SA*) is presented.

2. THEORETICAL BACKGROUND

In this paper, a muffler with reverse-flow perforated mufflers was adopted for noise elimination in the blower room shown in Fig. 1. The outlines of these mufflers are shown in Fig. 2. Before the acoustical fields of mufflers are analyzed, the acoustical elements have to be distinguished. As shown in Fig. 1, two kinds of muffler components, including two straight ducts and a reverse-flow perforated duct, are identified and symbolized as I and II. In addition, the acoustic pressure $\bar{p}$ and acoustic particle velocity $\bar{u}$ within the muffler are depicted in Fig. 2 where the acoustical field is represented by four nodes (node 1, 2, 4, and 5).

The muffler system is composed of two kinds of acoustical elements. The individual transfer matrix derivations with respect to two kinds of acoustical mechanisms are described below.

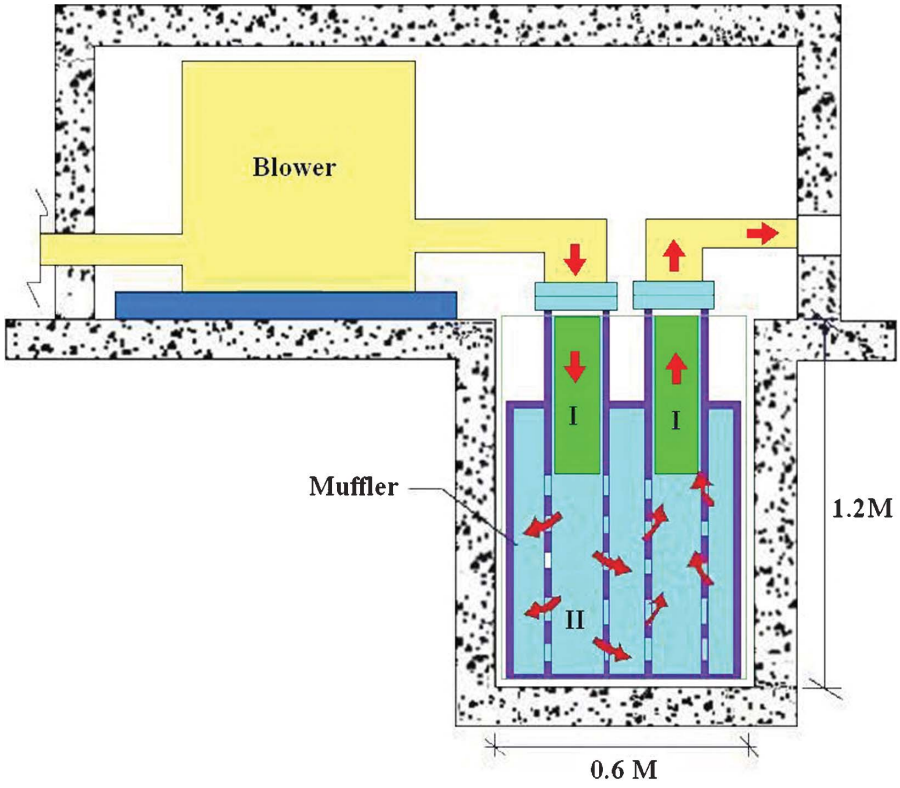

Fig. 1. A distinction in a muffler with reverse-flow ducts installed in a space-constrained blower room.

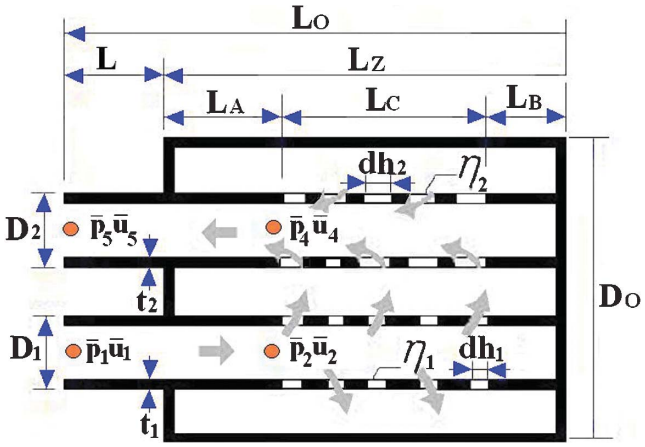

Fig. 2. The outline and acoustical field of a muffler with reverse-flow ducts.

2.1. System Matrix

Based on plane wave theory, the four-pole transfer matrix for a straight duct between nodes 1 and 2 is [14]

$$\begin{pmatrix} \bar{p}_1 \\ \rho_o c_o \bar{u}_1 \end{pmatrix} = e^{-j\frac{M_1 kL_1}{1-M_1^2}} \begin{bmatrix} TS1_{1,1} & TS1_{1,2} \\ TS1_{2,1} & TS1_{2,2} \end{bmatrix} \begin{pmatrix} \bar{p}_2 \\ \rho_o c_o \bar{u}_2 \end{pmatrix} \tag{1a}$$

where

$$\begin{aligned} &TS1_{1,1} = \cos\left[\frac{k(L_1+L_A)}{1-M_1^2}\right];\ TS1_{1,2} = j\sin\left[\frac{k(L_1+L_A)}{1-M_1^2}\right];\ TS1_{2,1} = j\sin\left[\frac{k(L_1+L_A)}{1-M_1^2}\right]; \\ &TS1_{2,2} = \cos\left[\frac{k(L_1+L_A)}{1-M_1^2}\right] \end{aligned} \tag{1b}$$

Similarly, the relationship between nodes 4 and 5 is

$$\begin{pmatrix} \bar{p}_4 \\ \rho_o c_o \bar{u}_4 \end{pmatrix} = e^{-j\frac{M_4 k(L_1+L_A)}{1-M_4^2}} \begin{bmatrix} TS3_{1,1} & TS3_{1,2} \\ TS3_{2,1} & TS3_{2,2} \end{bmatrix} \begin{pmatrix} \bar{p}_5 \\ \rho_o c_o \bar{u}_5 \end{pmatrix} \tag{2a}$$

where

$$\begin{aligned} &TS3_{1,1} = \cos\left[\frac{k(L_1+L_A)}{1-M_4^2}\right];\ TS3_{1,2} = j\sin\left[\frac{k(L_1+L_A)}{1-M_4^2}\right];\ TS3_{2,1} = j\sin\left[\frac{k(L_1+L_A)}{1-M_4^2}\right]; \\ &TS3_{2,2} = \cos\left[\frac{k(L_1+L_A)}{1-M_4^2}\right] \end{aligned} \tag{2b}$$

As derived in Appendix A, on the basis of plane wave theory, the four-pole transfer matrix for a reverse-flow perforated duct between nodes 2 and 4 is

$$\begin{bmatrix} \bar{p}_2 \\ \rho_o c_o \bar{u}_2 \end{bmatrix} = \begin{bmatrix} TPRF2_{1,1} & TPRF2_{1,2} \\ TPRF2_{2,1} & TPRF2_{2,2} \end{bmatrix} \begin{bmatrix} \bar{p}_4 \\ \rho_o c_o \bar{u}_4 \end{bmatrix} \tag{3}$$

The total transfer matrix assembled by multiplication from Eqs. (1)~(3) is

$$\begin{aligned} &\begin{pmatrix} \bar{p}_1 \\ \rho_o c_o \bar{u}_1 \end{pmatrix} \\ &= e^{-jk\left[\frac{M_1(L_1+L_A)}{1-M_1^2}+\frac{M_4(L_1+L_A)}{1-M_4^2}\right]} \begin{bmatrix} TS1_{1,1} & TS1_{1,2} \\ TS1_{2,1} & TS1_{2,2} \end{bmatrix} \begin{bmatrix} TPFR2_{1,1} & TPRF2_{1,2} \\ TPRF2_{2,1} & TPRF2_{2,2} \end{bmatrix} \\ &\begin{bmatrix} TS3_{1,1} & TS3_{1,2} \\ TS3_{2,1} & TS3_{2,2} \end{bmatrix} \begin{pmatrix} \bar{p}_5 \\ \rho_o c_o \bar{u}_5 \end{pmatrix} \end{aligned} \tag{4}$$

A simplified form in the matrix is expressed as

$$\begin{pmatrix} \bar{p}_1 \\ \rho_o c_o \bar{u}_1 \end{pmatrix} = \begin{bmatrix} T_{11}^* & T_{12}^* \\ T_{21}^* & T_{22}^* \end{bmatrix} \begin{pmatrix} \bar{p}_5 \\ \rho_o c_o \bar{u}_5 \end{pmatrix} \tag{5}$$

Under the assumption of a fixed thickness of the tubes (t_1=t_2=0.001 m) and the symmetric design (L_A=L_B=(L_Z-L_C)/2), the sound transmission loss (STL) of a muffler is defined as [14]

$$\begin{aligned} &STL(Q, f, RT_1, RT_2, RT_3, RT_4, dh_1, \eta_1, dh_2, \eta_2) \\ &= \log\left(\frac{\left|T_{11}^* + T_{12}^* + T_{21}^* + T_{22}^*\right|}{2}\right) + 10\log\left(\frac{S_1}{S_5}\right) \end{aligned} \tag{6a}$$

where

$$\begin{aligned} &RT_1 = L_Z/L_o;\ RT_2 = L_C/L_Z; RT_3 = D_1/D_o;\ RT_4 = D_2/D_o; \\ &L_o = L_1 + L_Z;\ L_Z = L_A + L_B + L_C; L_A = L_B = (L_Z - L_C)/2 \end{aligned} \tag{6b}$$

2.2. Overall Sound Power Level

The silenced octave sound power level emitted from a silencer's outlet is

$$SWL_i = SWLO_i - STL_i \tag{7}$$

where (1) $SWLO_i$ is the original SWL at the inlet of a muffler (or pipe outlet), and i is the index of the octave band frequency.

(2) STL_i is the muffler's STL with respect to the relative octave band frequency.

(3) SWL_i is the silenced SWL at the outlet of a muffler with respect to the relative octave band frequency.

Finally, the overall SWL_T silenced by a muffler at the outlet is

$$SWL_T = 10 * \log\left\{\sum_{i=1}^{6} 10^{SWL_i/10}\right\}$$
$$= 10 * \log\left\{\begin{array}{l} 10^{[SWLO(f=125)-STL(f=125)]/10} + 10^{[SWLO(f=250)-STL(f=250)]/10} + 10^{[SWLO(f=500)-STL(f=500)]/10} \\ + 10^{[SWLO(f=1000)-STL(f=1000)]/10} + 10^{[SWLO(f=2000)-STL(f=2000)]/10} \\ + 10^{[SWL(f=4000)-STL(f=4000)]/10} \end{array}\right\} \quad (8)$$

2.3. Objective Function

By using the formulas of Eqs. (6) and (8), the objective function used in the *SA* optimization was established.

STL Maximization for a One-tone (f) Noise:

$$OBJ_1 = STL(Q, f, RT_1, RT_2, RT_3, RT_4, dh_1, \eta_1, dh_2, \eta_2) \quad (9)$$

SWL Minimization for a Broadband Noise:

To minimize the overall SWL_T, the objective function is

$$OBJ_2 = SWL_T(Q, RT_1, RT_2, RT_3, RT_4, dh_1, \eta_1, dh_2, \eta_2) \quad (10)$$

3. MODEL CHECK

Before performing the *SA* optimal simulation on mufflers, an accuracy check of the mathematical model on a muffler with reverse-flow perforated tubes was performed by Munjal *et al.* [8]. As indicated in Fig. 3, the accuracy comparisons between theoretical data and

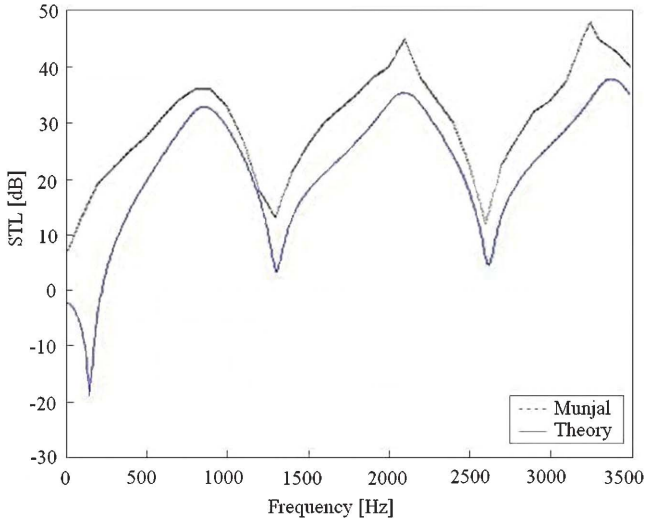

Fig. 3. Performance of a one-chamber reverse-flow perforated muffler [D_1=0.0493(m), D_1=0.0493(m), Do=0.1481(m), L_A=L_B=0.0064, L_c=0.1286(m), t_1=t_2=0.0081(m), dh_1=dh_2=0.0035(m), η_1=η_2=0.039, M_1=0.1], [Analytical data is from Munjal *et al.* [8]].

Table 1. The spectrum of exhaust sound power levels (*SWL*s).

f(Hz)	125	250	500	1k	2k	4k	Overall
SWLO-dB	130	140	128	115	110	105	140.7

analytical data are in agreement. Therefore, the mathematic model of mufflers with reverse-flow and perforated tubes is acceptable and adopted in the following optimization process.

4. CASE STUDIES

In this paper, the noise reduction of a space-constrained blower is exemplified and shown in Fig. 1. The sound power level (*SWL*) inside the blower's outlet is shown in Table 1 where the overall *SWL* reaches 140.7 dB. To depress the huge exhaust noise emitted from the blower's outlet, a muffler hybridized with reverse-flow tubes installed under the ground is considered.

To obtain the best acoustical performance within a fixed space volume, numerical assessments linked to a *S*A optimizer are applied. Before the minimization of a broadband noise is executed, a reliability check of the *SA* method by maximization of the *STL* at one targeted tone (300 Hz) has been carried out. As shown in Figs. 1 and 2, the available space for a muffler is 0.6 m in width, 0.6 m in height, and 1.2 m in length. The flow rate (Q) and thickness of a perforated tube (t) are preset as 0.05 (m^3/s) and 0.001(m), respectively. The corresponding *OBJ* functions, space constraints, and the ranges of design parameters are summarized in Table 2.

5. SIMULATED ANNEALING

The basic concept behind *SA* was first introduced by Metropolis *et al.* [15] and developed by Kirkpatrick *et al.* [16]. SA simulates the annealing of metal. Annealing is the process of heating and keeping a metal at a stabilized temperature while cooling it slowly. Slow cooling allows the particles to attain their state close to the minimal energy state. The algorithm starts by generating a random initial solution. The scheme of the *SA* is a variation of the hill-climbing algorithm. All downhill movements for improvement are accepted for the decrement of the system's energy. The purpose of *SA* is to avoid stacking in local optimal solutions during optimization. In order to escape from the local optimum, the *SA* also allows movements resulting in solutions that are worse (uphill moves) than the current solution. To imitate the evolution of the *SA* algorithm, a new random solution (X') is chosen from the neighborhood of the current solution (X). If the change in objective function (or energy) is negative ($\Delta F \leq 0$), the new solution will be accepted as the new current solution with the transition property $pb(X') = 1$. If the change is not negative ($\Delta F > 0$), the new transition property $pb(X')$ will be computed by the Boltzmann's factor $pb(X') = \exp(\Delta F/CT)$ as the Eq. (11)

Table 2. Range of design parameters for a muffler with reverse-flow ducts.

	Range of design parameters
A muffler with reverse-flow ducts	Targeted f =300 (Hz); Q=0.05 (m^3/s); L_o=1.2 (m); D_o=0.6 (m) RT_1:[0.5, 0.9]; RT_2:[0.1, 0.9]; RT_3:[0.1, 0.4]; RT_4:[0.1, 0.4]; η_1: [0. 03, 0.1]; dh_1:[0. 00175, 0.007]; η_2:[0. 03, 0.1]; dh_2:[0. 00175, 0.007];

$$pb(X') = \begin{cases} 1, \Delta F \le 0 \\ \exp\left(\dfrac{-\Delta F}{CT}\right), \Delta f > 0 \end{cases} \tag{11a}$$

$$\Delta F = F(X') - F(X) \tag{11b}$$

where C and T are the Boltzmann constant and the current temperature. Moreover, compared with the new random probability of rand(0,1), each successful substitution of the new current solution will lead to the decay of the current temperature as

$$T_{new} = kk * T_{old}$$

where kk is the cooling rate. The process is repeated until the predetermined number (*Iter*) of the outer loop is reached.

The flow diagram of the *SA* optimization is described and shown in Fig. 4.

6. RESULTS AND DISCUSSION

6.1. Results

The accuracy of the *SA* optimization depends on the cooling rate (*kk*) and the number of iterations (*Iter*). To achieve good optimization, both the cooling rate (*kk*) and the number of iterations (*Iter*) are varied step by step

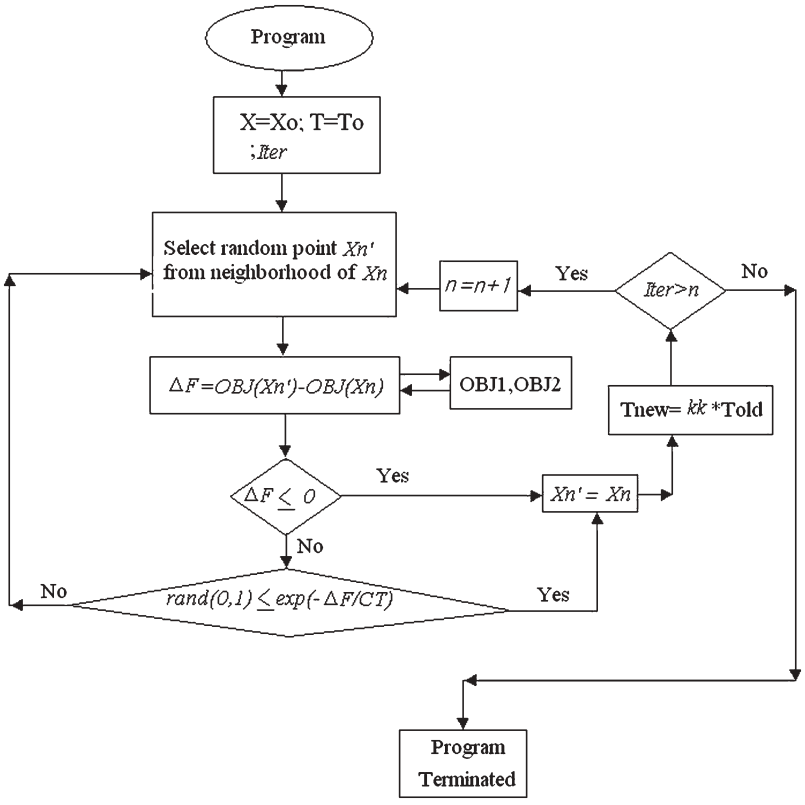

Fig. 4. Flow diagram of a *SA* optimization.

$$kk = (0.90,0.93,0.96,0.99);\ Iter = (50,200,800)$$

The results of two kinds of optimizations — one of the pure tone noise and the others of the broadband noise — are described below.

Pure Tone Noise Optimization:

Six sets of *SA* parameters are tested by varying the values of the *SA* parameters. The simulated results with respect to the pure tone of 300 Hz is summarized and shown in Table 3. As indicated in Table 3, the optimal design data can be obtained from the last set of *SA* parameters at (*kk, Iter*) = (0.99, 800). Using the optimal design in a theoretical calculation, the optimal *STL* curves with respect to various *SA* parameters are plotted and depicted in Fig. 5. As revealed in Fig. 5, the optimal *STL* is maximized at the desired frequency.

Table 3. Optimal *STL* for a muffler with reverse-flow ducts (at a targeted tone of 300 Hz).

SA parameters		Results				
kk	*Iter*					
0.90	50	*RT*1	*RT*2	*RT*3	*RT*4	*STL* (dB)
		0.8997	0.8993	0.3997	0.3997	19.5
		η_1	dh_1(m)	η_2	dh_2(m)	
		0.006996	0.09994	0.006996	0.09994	
0.93	50	*RT*1	*RT*2	*RT*3	*RT*4	*STL* (dB)
		0.8785	0.8570	0.3839	0.3839	24.5
		η_1	dh_1(m)	η_2	dh_2(m)	
		0.006718	0.09623	0.006718	0.09623	
0.96	50	*RT*1	*RT*2	*RT*3	*RT*4	*STL* (dB)
		0.8657	0.8315	0.3743	0.3743	26.0
		η_1	dh_1(m)	η_2	dh_2(m)	
		0.006550	0.09400	0.006550	0.09400	
0.99	50	*RT*1	*RT*2	*RT*3	*RT*4	*STL* (dB)
		0.8405	0.7810	0.3554	0.3554	26.5
		η_1	dh_1(m)	η_2	dh_2(m)	
		0.006219	0.08959	0.006219	0.08959	
0.99	200	*RT*1	*RT*2	*RT*3	*RT*4	*STL* (dB)
		0.8241	0.7482	0.3431	0.3431	27.5
		η_1	dh_1(m)	η_2	dh_2(m)	
		0.006004	0.08672	0.006004	0.08672	
0.99	800	*RT*1	*RT*2	*RT*3	*RT*4	*STL* (dB)
		0.6875	0.4749	0.2406	0.2406	85.5
		η_1	dh_1(m)	η_2	dh_2(m)	
		0.004210	0.06281	0.004210	0.06281	

Notes: $RT_1 = L_Z/L_o$; $RT_2 = L_C/L_Z$; $RT_3 = D_1/D_o$; $RT_4 = D_2/D_o$; $L_o = L_1 + L_Z$; $L_Z = L_A + L_B + L_C$; $L_A = L_B = (L_Z - L_C)/2$.

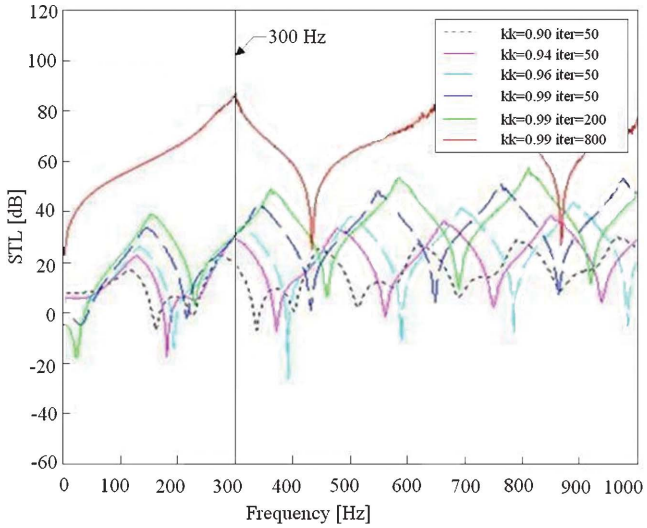

Fig. 5. The *STL* with respect to frequencies at various SA parameters (targeted tone: 300Hz).

Broadband Noise Optimization:

By using the above *SA* parameters, the muffler's optimal design data for mufflers hybridized with reverse-flow perforated ducts used to minimize the sound power level at the muffler's outlet is summarized in Table 4. As illustrated in Table 4, the resultant sound power levels have been dramatically reduced from 140.7 dB to 42.5 dB. Using this optimal design in a theoretical calculation, the resultant *SWL* before and after adding the muffler at the outlet is shown in Fig. 6. As shown in Fig. 6, the muffler has the best acoustical performance.

6.2. Discussion

To achieve a sufficient optimization, the selection of the appropriate *SA* parameter set is essential. As indicated in Table 3, the best *SA* set at the targeted pure tone noise of 300 Hz has

Table 4. Optimal *SWL* for a muffler with reverse-flow ducts (broadband noise).

Item	SA parameters		Results				
	kk	*Iter*					
1	0.99	50	*RT*1	*RT*2	*RT*3	*RT*4	SWL_T (dB)
			0.8227	0.7453	0.3420	0.3420	75.5
			η_1	dh_1(m)	η_2	dh_2(m)	
			0.005985	0.08647	0.005985	0.08647	
2	0.99	200	*RT*1	*RT*2	*RT*3	*RT*4	SWL_T (dB)
			0.8329	0.7657	0.3496	0.3496	71.9
			η_1	dh_1(m)	η_2	dh_2(m)	
			0.006119	0.08825	0.006119	0.08825	
3	0.99	800	*RT*1	*RT*2	*RT*3	*RT*4	SWL_T (dB)
			0.7007	0.5015	0.2506	0.2506	42.5
			η_1	dh_1(m)	η_2	dh_2(m)	
			0.004385	0.06513	0.004385	0.06513	

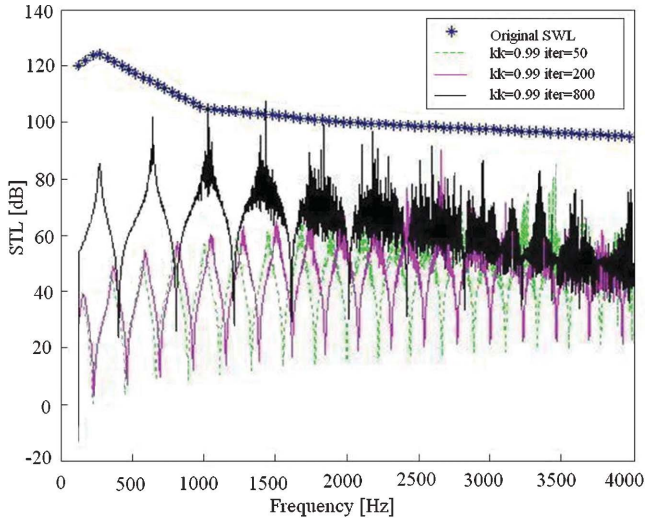

Fig. 6. Optimal *STL* for mufflers designed at various *SA* parameters (broadband noise).

been shown. Using the appropriate *SA* set at the targeted pure tone (300 Hz), the related optimal *STL* curves plotted in Fig. 5 reveals that the predicted maximal value of the *STL* is located at the desired frequency. Therefore, using the *SA* optimization in finding a better design solution has proven reliable; moreover, as can be seen in Fig. 5, not only the peak frequency of the STL profile is shifting toward the targeted tone but the peak value will increase when a better solution assessed in the SA optimization procedure. Meanwhile, all of the design data (RT_1, RT_2, RT_3, RT_4, η_1, dh_1, η_2, dh_2) were decrease. It means that the shorter of the length of the perforated tube and the smaller diameter and number of the perforated hole will result in a higher frequency. Besides, the STL will also increase when the diameter of the perforated tubes decrease.

7. CONCLUSION

It has been shown that mufflers hybridized with reversed-flow and perforated ducts can be easily and efficiently optimized within a limited space by using a generalized decoupling technique, a plane wave theory, a four-pole transfer matrix, as well as a *SA* optimizer. Two kinds of *SA* parameters (*kk, Iter*) play essential roles in the solution's accuracy during the *SA* optimization. As indicated in Fig. 5, the tuning ability established by adjusting design of the mufflers is reliable. In additional, the design data reveals that the peak frequency of the STL will shift rightward if the length of the perforated tube, the diameter of the perforated hole, and the number of the perforated hole decrease. Besides, the whole STL will increase if the diameter of the perforated tubes decreases. Subsequently, the appropriate acoustical performance curve of mufflers with reverse-flow and perforated ducts in depressing overall broadband noise have been assessed. As can be seen in Table 4 and Fig. 6, the overall sound power level (SWL_T) of a blower is minimized by adjusting an appropriate spectrum of the STL. Consequently, the approach used for the optimal design of the *STL* proposed in this study is indeed easy and quite effective.

ACKNOWLEDGEMENTS

The author acknowledges the financial support of the National Science Council (NSC 97-2622-E-235-002-CC3, Taiwan, ROC) and would also like to thank the anonymous referees who kindly provided the suggestions and comments to improve this work.

REFERENCES

1. Davis, D.D., Stokes, J.M., Moorse, L., ''Theoretical and experimental investigation of mufflers with components on engine muffler design,'' *NACA Report*, pp.1192, 1954.
2. Sullivan, J.W. and Crocker, M.J., ''Analysis of concentric tube resonators having unpartitioned cavities,'' *Acoustical Society of America*, Vol. 64, pp. 207–215, 1978.
3. Sullivan, J.W., ''A method of modeling perforated tube muffler components I: theory,'' *Acoustical Society of America*, Vol. 66, pp. 772–778, 1979.
4. Sullivan, J.W., ''A method of modeling perforated tube muffler components II: theory,'' *Acoustical Society of America*, Vol. 66, pp. 779–788, 1979.
5. Jayaraman, K. and Yam, K., ''Decoupling approach to modeling perforated tube muffler component,'' *Acoustical Society of America*, Vol. 69, No. 2, pp. 390–396, 1981.
6. Thawani, P.T. and Jayaraman, K., ''Modeling and applications of straight-through resonators,'' *Acoustical Society of America*, Vol. 73, No. 4, pp. 1387–1389, 1983.
7. Rao, K.N. and Munjal, M.L., ''A Generalized Decoupling Method for Analyzing Perforated Element Mufflers,'' Nelson Acoustics Conference, Madison, 1984.
8. Munjal, M.L., Rao, K.N. and Sahasrabudhe, A.D., ''Aeroacoustic analysis of perforated muffler components,'' *Journal of Sound and Vibration*, Vol. 114, No. 2, pp. 173–188, 1987.
9. Peat, K.S., ''A numerical decoupling analysis of perforated pipe silencer elements,'' *Journal of Sound and Vibration*, Vol. 123, No. 2, pp. 199–212, 1988.
10. Yeh, L.J., Chang, Y.C., Chiu, M.C. and Lai, G.J., ''Computer-aided optimal design of a single-chamber muffler with side inlet/outlet under space constraints,'' *Journal of Marine Science and Technology*, Vol. 11, No. 4, pp. 1–8, 2003.
11. Chang, Y.C., Yeh, L. J. and Chiu, M.C., ''Numerical studies on constrained venting system with side inlet/outlet mufflers by GA optimization,'' *Acta Acustica united with Acustica*, Vol. 90, pp. 1–11, 2004.
12. Chang, Y.C., Yeh, L.J. and Chiu, M.C., ''Shape optimization on double-chamber mufflers using genetic algorithm,'' *Proc. ImechE Part C: Journal of Mechanical Engineering Science*, Vol. 10, pp. 31–42, 2005.
13. Yeh, L.J., Chang, Y.C. and Chiu, M.C., ''Numerical studies on constrained venting system with reactive mufflers by GA optimization,'' *International Journal for Numerical Methods in Engineering*, Vol. 65, pp. 1165–1185, 2006.
14. Munjal, M.L. ''*Acoustics of Ducts and Mufflers with Application to Exhaust and Ventilation System Design*,'' New York: John Wiley & Sons, 1987.
15. Metropolis, A., Rosenbluth, W., Rosenbluth, M. N., Teller, H. and Teller, E., ''Equation of static calculations by fast computing machines,'' *The Journal of Chemical Physics*, Vol. 21, pp. 1087–1092, 1953.
16. Kirkpatrick, S., Gelatt, C.D. and Vecchi, M.P., ''Optimization by simulated annealing,'' *Science*, Vol. 220, pp. 671–680, 1983.
17. Rao, K.N. and Munjal, M.L., ''Experimental evaluation of impedance of perforates with grazing flow,'' *Journal of Sound and Vibration*, Vol. 123, pp. 283–295, 1986.

APPENDIX A-TRANSFER MATRIX OF A REVERSE-FLOW PERFORATED DUCT

As shown in Fig. 7, there are six nodes located inside the acoustical field. Based on the derivation from Munjal *et al.* [14], the continuity equations and momentum equations with respect to the inner and outer tubes in the first chamber are listed below.

Inner tube 1:

continuity equation

$$V_2\frac{\partial \rho_2}{\partial x}+\rho_o\frac{\partial u_2}{\partial x}+\frac{4\rho_o}{D_1}u_{2,3}+\frac{\partial \rho_2}{\partial t}=0 \tag{A1}$$

momentum equation

$$\rho_o\left(\frac{\partial}{\partial t}+V_2\frac{\partial}{\partial x}\right)u_2+\frac{\partial p_2}{\partial x}=0 \tag{A2}$$

Inner tube 2:

continuity equation

$$V_4\frac{\partial \rho_4}{\partial x}+\rho_o\frac{\partial u_4}{\partial x}-\frac{4\rho_o}{D_8}u_{3,4}+\frac{\partial \rho_4}{\partial t}=0 \tag{A3}$$

momentum equation

$$\rho_o\left(\frac{\partial}{\partial t}+V_4\frac{\partial}{\partial x}\right)u_4+\frac{\partial p_4}{\partial x}=0 \tag{A4}$$

Outer tube:

continuity equation

$$\rho_o\frac{\partial u_3}{\partial x}-V_3\frac{\partial \rho_3}{\partial x}-\frac{4D_1\rho_o}{D_o^2-D_1^2-D_2^2}u_{2,3}+\frac{4D_2}{D_o^2-D_1^2-D_2^2}\rho_o u_{2,3}+\frac{\partial \rho_3}{\partial t}=0 \tag{A5}$$

momentum equation

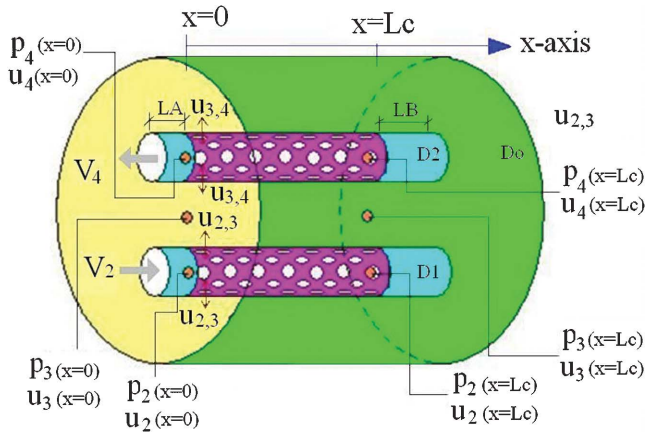

Fig. 7. The mechanism of an acoustical element for a muffler with reverse -flow perforated ducts.

$$\rho_o\left(\frac{\partial}{\partial t}+V_3\frac{\partial}{\partial x}\right)u_3+\frac{\partial \rho_3}{\partial x}=0 \tag{A6}$$

Assuming that the acoustic wave is a harmonic motion

$$p(x,t)=P(x)\cdot e^{j\omega t} \tag{A7}$$

under the isentropic processes in ducts, it yields

$$P(x)=\rho(x)\cdot c_o^2 \tag{A8}$$

Assuming that the perforation along the inner tubes is uniform (ie.$d\xi/dx=0$), the acoustic impedance of the perforation ($\rho_o c_o \xi$) is

$$\rho_o c_o \xi_1=\frac{p_2(x)-p_3(x)}{u_{2,3}(x)} \tag{A9}$$

$$\rho_o c_o \xi_2=\frac{p_2(x)-p_3(x)}{u_{2,3}(x)} \tag{A10}$$

where ξ_1,ξ_2 are the specific acoustical impedances of the inner perforated tube1 and tube 2, respectively. According to the formula of ξ developed by Sullivan [3] and Rao [17], the empirical formulations for the perforation with or without mean flow are adopted in this study.

For perforates with stationary medium, we have

$$\xi_1=[0.006+jk(t_1+0.75dh_1)]/\eta_1 \tag{A11a}$$

$$\xi_2=[0.006+jk(t_2+0.75dh_2)]/\eta_2 \tag{A11b}$$

For perforates with grazing flow, we have

$$\xi_1=[0.514D_1M_2/(L_C\eta_1)+j0.95k(t_1+0.75dh_1)]/\eta_1 \tag{A12a}$$

$$\xi_2=[0.514D_3M_4/(L_C\eta_2)+j0.95k(t_2+0.75dh_2)]/\eta_2 \tag{A12b}$$

where dh_1 and dh_2 are the diameters of the perforated holes on the inner tube 1 and the tube 2; t_1 and t_2 are the thicknesses of the inner perforated tube 1 and tube 2; η_1 and η_2 are the porosities of the perforated tube 1 and tube 2.

The available ranges of the above parameters are [17]

$$\mathrm{M}: \ 0.05 \leqq \mathrm{M}_2, \ \mathrm{M}_4 \leqq 0.2 \tag{A13a}$$

$$\eta: \ 0.03 \leqq \eta_1, \eta_2 \leqq 0.1 \tag{A13b}$$

$$\mathrm{t}: \ 0.001 \leqq \mathrm{t}_1, \ \mathrm{t}_2 \leqq 0.003 \tag{A13c}$$

$$\mathrm{dh}: \ 0.00175 \leqq dh_1, dh_2 \leqq 0.007 \tag{13d}$$

Eliminating u_2,u_4,$u_{2,3}$,$u_{3,4}$,ρ_2,ρ_3 and ρ_4 yields

$$\begin{bmatrix} D^2+\alpha_1 D+\alpha_2 & \alpha_3 D+\alpha_4 & 0 \\ \alpha_5 D+\alpha_6 & D^2+\alpha_7 D+\alpha_8 & \alpha_9 D+\alpha_{10} \\ 0 & \alpha_{11} D+\alpha_{12} & D^2+\alpha_{13} D+\alpha_{14} \end{bmatrix} \begin{bmatrix} p_2(x) \\ p_3(x) \\ p_4(x) \end{bmatrix} = \begin{bmatrix} 0 \\ 0 \\ 0 \end{bmatrix} \tag{A14}$$

Developing Eq.(A14) yields

$$p_2'' + \alpha_1 p_2' + \alpha_2 p_2 + \alpha_3 p_3' + \alpha_4 p_3 = 0 \tag{A15a}$$

$$\alpha_5 p_2' + \alpha_6 p_2 + p_3'' + \alpha_7 p_3' + \alpha_8 p_3 + \alpha_9 p_4' + \alpha_{10} p_4 = 0 \tag{A15b}$$

$$\alpha_{11} p_3' + \alpha_{12} p_3 + p_4'' + \alpha_{13} p_4' + \alpha_{14} p_4 = 0 \tag{A15c}$$

where

$$\begin{aligned}
&D = \frac{d}{dx}; \ \alpha_1 = -\frac{jM_2}{1-M_2^2}\left(2k - j\frac{4}{D_1\xi_1}\right); \ \alpha_2 = \frac{1}{1-M_2^2}\left(k^2 - j\frac{4k}{D_1\xi_1}\right); \\
&\alpha_3 = \frac{M_2}{1-M_2^2}\cdot\frac{4}{D_1\xi_1}; \ \alpha_4 = -\frac{j}{1-M_2^2}\cdot\frac{4k}{D_1\xi_1}; \ \alpha_5 = \frac{M_3}{1-M_3^2}\cdot\frac{4D_1}{(D_o^2-D_1^2-D_2^2)\xi_1}; \\
&\alpha_6 = \frac{j}{1-M_3^2}\cdot\frac{4kD_1}{(D_o^2-D_1^2-D_2^2)\xi_1}; \ \alpha_7 = -\frac{jM_3}{1-M_3^2}\left(2k - \frac{j4D_1}{(D_o^2-D_1^2-D_2^2)\xi_1} - \frac{j4D_2}{(D_o^2-D_1^2-D_2^2)\xi_2}\right); \\
&\alpha_8 = \frac{1}{1-M_3}\left(k^2 - \frac{j4kD_1}{(D_o^2-D_1^2-D_2^2)\xi_1} - \frac{j4kD_2}{(D_o^2-D_1^2-D_2^2)\xi_2}\right); \\
&\alpha_9 = \frac{M_3}{1-M_3^2}\left(\frac{4D_2}{(D_o^2-D_1^2-D_2^2)\xi_2}\right); \alpha_{10} = \frac{j}{1-M_3^2}\left(\frac{4kD_2}{(D_o^2-D_1^2-D_2^2)\xi_2}\right); \\
&\alpha_{11} = \frac{M_4}{1-M_4^2}\left(\frac{4}{D_2\xi_2}\right); \ \alpha_{12} = \frac{j}{1-M_4^2}\left(\frac{4k}{D_2\xi_2}\right); \alpha_{13} = \frac{-jM_4}{1-M_4^2}\left(2k - j\frac{4}{D_2\xi_2}\right); \\
&\alpha_{14} = \frac{1}{1-M_4^2}\left(k^2 - j\frac{4k}{D_2\xi_2}\right);
\end{aligned} \tag{A15d}$$

Let $p_2' = \dfrac{dp_2}{dx} = y_1$, $p_3' = \dfrac{dp_3}{dx} = y_2$, $p_4' = \dfrac{dp_4}{dx} = y_3$, $p_2 = y_4$, $p_3 = y_5$, $p_4 = y_6$

The new matrix between {y'} and {y} is

$$\begin{bmatrix} y_1' \\ y_2' \\ y_3' \\ y_4' \\ y_5' \\ y_6' \end{bmatrix} = \begin{bmatrix} -\alpha_1 & -\alpha_3 & 0 & -\alpha_2 & -\alpha_4 & 0 \\ -\alpha_5 & -\alpha_7 & -\alpha_9 & -\alpha_6 & -\alpha_8 & -\alpha_{10} \\ 0 & -\alpha_{11} & -\alpha_{13} & 0 & -\alpha_{12} & -\alpha_{14} \\ 1 & 0 & 0 & 0 & 0 & 0 \\ 0 & 1 & 0 & 0 & 0 & 0 \\ 0 & 0 & 1 & 0 & 0 & 0 \end{bmatrix} \begin{bmatrix} y_1 \\ y_2 \\ y_3 \\ y_4 \\ y_5 \\ y_6 \end{bmatrix} \tag{A16a}$$

which can be briefly expressed as

$$\{y'\} = [\Lambda\Lambda]\{y\} \tag{A16b}$$

Let

$$\{y\} = \begin{bmatrix} dp_2/dx \\ dp_3/dx \\ dp_4/dx \\ p_2 \\ p_3 \\ p_4 \end{bmatrix} = \begin{bmatrix} \Pi\Pi_{1,1} & \Pi\Pi_{1,2} & \Pi\Pi_{1,3} & \Pi\Pi_{1,4} & \Pi\Pi_{1,5} & \Pi\Pi_{1.6} \\ \Pi\Pi_{2,1} & \Pi\Pi_{2,2} & \Pi\Pi_{2,3} & \Pi\Pi_{2,4} & \Pi\Pi_{2,5} & \Pi\Pi_{2,6} \\ \Pi\Pi_{3,1} & \Pi\Pi_{3,2} & \Pi\Pi_{3,3} & \Pi\Pi_{3,4} & \Pi\Pi_{3,5} & \Pi\Pi_{3,6} \\ \Pi\Pi_{4,1} & \Pi\Pi_{4,2} & \Pi\Pi_{4,3} & \Pi\Pi_{4,4} & \Pi\Pi_{4,5} & \Pi\Pi_{4,6} \\ \Pi\Pi_{5,1} & \Pi\Pi_{5,2} & \Pi\Pi_{5,3} & \Pi\Pi_{5,4} & \Pi\Pi_{5,5} & \Pi\Pi_{5,6} \\ \Pi\Pi_{6,1} & \Pi\Pi_{6,2} & \Pi\Pi_{6,3} & \Pi\Pi_{6,4} & \Pi\Pi_{6,5} & \Pi\Pi_{6,6} \end{bmatrix} \begin{bmatrix} \Gamma\Gamma_1 \\ \Gamma\Gamma_2 \\ \Gamma\Gamma_3 \\ \Gamma\Gamma_4 \\ \Gamma\Gamma_5 \\ \Gamma\Gamma_6 \end{bmatrix} \tag{A17}$$

where $[\Pi\Pi]_{6x6}$ is the modal matrix formed by six sets of eigen vectors $\Pi\Pi_{6x1}$ of $[\Lambda\Lambda]_{6x6}$.

Combining Eq.(A17) with (A16) and then multiplying $[\Pi\Pi]^{-1}$ by both sides, we have

$$[\Pi\Pi]^{-1}[\Pi\Pi]\{\Gamma\Gamma'\} = [\Pi\Pi]^{-1}[\Lambda\Lambda][\Pi\Pi]\{\Gamma\Gamma\} \tag{A18}$$

$$\text{Set } [\Omega\Omega] = [\Pi\Pi]^{-1}[\Lambda\Lambda][\Pi\Pi] = \begin{bmatrix} \lambda_1 & 0 & 0 & 0 & 0 & 0 \\ 0 & \lambda_2 & 0 & 0 & 0 & 0 \\ 0 & 0 & \lambda_3 & 0 & 0 & 0 \\ 0 & 0 & 0 & \lambda_4 & 0 & 0 \\ 0 & 0 & 0 & 0 & \lambda_5 & 0 \\ 0 & 0 & 0 & 0 & 0 & \lambda_6 \end{bmatrix} \tag{A19}$$

where λ_i is the eigen value of $[\Lambda\Lambda]$.

Eq.(A17) can be thus rewritten as

$$\left\{\Gamma\Gamma'\right\} = [\Omega\Omega]\{\Gamma\Gamma\} \tag{A20}$$

Obviously, Eq.(20) is a decoupled equation. The related solution yields

$$\Gamma\Gamma_i = kf_i e^{\lambda_i x} \tag{A21}$$

Using Eqs.(A2),(A4),(A6),(A17) and (A21), the relationship of the acoustic pressure and the particle velocity yields

$$\begin{bmatrix} p_2(x) \\ p_3(x) \\ p_4(x) \\ \rho_o c_o u_2(x) \\ \rho_o c_o u_3(x) \\ \rho_o c_o u_4(x) \end{bmatrix} = \begin{bmatrix} \mathrm{E}_{1,1} & \mathrm{E}_{1,2} & \mathrm{E}_{1,3} & \mathrm{E}_{1,4} & \mathrm{E}_{1,5} & \mathrm{E}_{1,6} \\ \mathrm{E}_{2,1} & \mathrm{E}_{2,2} & \mathrm{E}_{2,3} & \mathrm{E}_{2,4} & \mathrm{E}_{2,5} & \mathrm{E}_{2,6} \\ \mathrm{E}_{3,1} & \mathrm{E}_{3,2} & \mathrm{E}_{3,3} & \mathrm{E}_{3,4} & \mathrm{E}_{3,5} & \mathrm{E}_{3,6} \\ \mathrm{E}_{4,1} & \mathrm{E}_{4,2} & \mathrm{E}_{4,3} & \mathrm{E}_{4,4} & \mathrm{E}_{4,5} & \mathrm{E}_{4,6} \\ \mathrm{E}_{5,1} & \mathrm{E}_{5,2} & \mathrm{E}_{5,3} & \mathrm{E}_{5,4} & \mathrm{E}_{5,5} & \mathrm{E}_{5,6} \\ \mathrm{E}_{6,1} & \mathrm{E}_{6,2} & \mathrm{E}_{6,3} & \mathrm{E}_{6,4} & \mathrm{E}_{6,5} & \mathrm{E}_{6,6} \end{bmatrix} \begin{bmatrix} kf_1 \\ kf_2 \\ kf_3 \\ kf_4 \\ kf_5 \\ kf_6 \end{bmatrix} \tag{A22a}$$

where

$$\begin{aligned} &E_{1,i} = \Pi\Pi_{4,i} e^{\lambda_i x};\ E_{2,i} = \Pi\Pi_{5,i} e^{\lambda_i x};\ E_{3,i} = \Pi\Pi_{6,i} e^{\lambda_i x};\ E_{4,i} = -\frac{\Pi\Pi_{1,i} e^{\lambda_i x}}{jk + M_2\lambda_i}; \\ &E_{5,i} = -\frac{\Pi\Pi_{2,i} e^{\lambda_i x}}{jk + M_3\lambda_i};\ E_{6,i} = -\frac{\Pi\Pi_{3,i} e^{\lambda_i x}}{jk + M_4\lambda_i} \end{aligned} \tag{A22b}$$

Plugging x=0 and x=Lc into Eq.(A22) and doing rearrangement yield

$$\begin{bmatrix} p_2(0) \\ p_3(0) \\ p_4(0) \\ \rho_o c_o u_2(0) \\ \rho_o c_o u_3(0) \\ \rho_o c_o u_4(0) \end{bmatrix} = [\mathrm{Y}] \begin{bmatrix} p_2(L_C) \\ p_3(L_C) \\ p_4(L_C) \\ \rho_o c_o u_2(L_C) \\ \rho_o c_o u_3(L_C) \\ \rho_o c_o u_4(L_C) \end{bmatrix} \tag{A23a}$$

where

$$[\mathrm{Y}] = [\mathrm{E}(0)][\mathrm{E}(L_C)]^{-1} \tag{A23b}$$

To obtain the transform matrix between the inlet (x=0) and the outlet (x=Lc) of the inner tubes, four boundary conditions for the outer tube at x=0 and x=Lc are placed in the calculation.

$$\frac{p_3(0)}{-u_3(0)} = -j\rho_o c_o \cot(kL_A) \tag{A24a}$$

$$\frac{p_2(L_C)}{u_2(L_C)} = -j\rho_o c_o \cot(kL_B) \tag{A24b}$$

$$\frac{p_3(L_C)}{u_3(L_C)} = -j\rho_o c_o \cot(kL_B) \tag{A24c}$$

$$\frac{p_4(L_C)}{u_4(L_C)} = -j\rho_o c_o \cot(kL_B) \tag{A24d}$$

By combining Eqs.(A23a, b, c, d) with Eq.(A24) and developing them, the transfer matrix yields

$$\begin{bmatrix} p_2(0) \\ \rho_o c_o u_2(0) \end{bmatrix} = \begin{bmatrix} TPRF2_{1,1} & TPRF2_{1,2} \\ TPRF2_{2,1} & TPRF2_{2,2} \end{bmatrix} \begin{bmatrix} p_4(L_C) \\ \rho_o c_o u_4(L_C) \end{bmatrix} \tag{A25a}$$

or in a brief form

$$\begin{bmatrix} \bar{p}_2 \\ \rho_o c_o \bar{u}_2 \end{bmatrix} = \begin{bmatrix} TPRF2_{1,1} & TPRF2_{1,2} \\ TPRF2_{2,1} & TPRF2_{2,2} \end{bmatrix} \begin{bmatrix} \bar{p}_4 \\ \rho_o c_o \bar{u}_4 \end{bmatrix} \tag{A25b}$$

where

$$\bar{p}_2 = p_2(0);\ \bar{u}_2 = u_2(0);\ \bar{p}_4 = p_4(L_C);\ \bar{u}_4 = -u_4(L_C);$$

$$TPRF2_{1,1} = \frac{H_{15}}{H_{17}};\ TPRF2_{1,2} = \frac{1}{\rho_o c_o}\cdot\left(\frac{H_{15}H_{18}}{H_{17}} - H_{16}\right);\ TPRF2_{2,1} = \frac{\rho_o c_o}{H_{17}};$$

$$TPRF2_{2,2} = \frac{H_{18}}{H_{19}};$$

$$K_{11} = \rho_o c_o[\mathrm{Y}_{14} - j\mathrm{Y}_{11}\cot(kL_B)];\ K_{12} = \rho_o c_o[\mathrm{Y}_{15} - j\mathrm{Y}_{12}\cot(kL_B)];$$

$$K_{13} = \rho_o c_o[\mathrm{Y}_{16} - j\mathrm{Y}_{13}\cot(kL_B)];\ K_{21} = \rho_o c_o[\mathrm{Y}_{24} - j\mathrm{Y}_{21}\cot(kL_B)];$$

$$K_{22} = \rho_o c_o[\mathrm{Y}_{25} - j\mathrm{Y}_{22}\cot(kL_B)];\ K_{23} = \rho_o c_o[\mathrm{Y}_{26} - j\mathrm{Y}_{23}\cot(kL_B)];$$

$$K_{31} = \rho_o c_o[\mathrm{Y}_{34} - j\mathrm{Y}_{31}\cot(kL_B)];\ K_{32} = \rho_o c_o[\mathrm{Y}_{35} - j\mathrm{Y}_{32}\cot(kL_B)];$$

$$K_{33} = \rho_o c_o[\mathrm{Y}_{36} - j\mathrm{Y}_{33}\cot(kL_B)];\ K_{41} = \rho_o c_o[\mathrm{Y}_{44} - j\mathrm{Y}_{41}\cot(kL_B)];$$

$$K_{42} = \rho_o c_o[\mathrm{Y}_{45} - j\mathrm{Y}_{42}\cot(kL_B)];\ K_{43} = \rho_o c_o[\mathrm{Y}_{46} - j\mathrm{Y}_{43}\cot(kL_B)];$$

$$K_{51} = \rho_o c_o[\mathrm{Y}_{54} - j\mathrm{Y}_{51}\cot(kL_B)];\ K_{52} = \rho_o c_o[\mathrm{Y}_{55} - j\mathrm{Y}_{52}\cot(kL_B)]; \tag{A25c}$$

$$K_{53} = \rho_o c_o[\mathrm{Y}_{56} - j\mathrm{Y}_{53}\cot(kL_B)];\ K_{61} = \rho_o c_o[\mathrm{Y}_{64} - j\mathrm{Y}_{61}\cot(kL_B)];$$

$$K_{62} = \rho_o c_o[\mathrm{Y}_{65} - j\mathrm{Y}_{62}\cot(kL_B)];\ K_{63} = \rho_o c_o[\mathrm{Y}_{66} - j\mathrm{Y}_{63}\cot(kL_B)];$$

$$H_1 = \frac{j\cot(kL_A)\cdot K_{52} - K_{22}}{K_{21} - jK_{51}\cot(kL_A)};\ H_2 = \frac{j\cot(kL_A)\cdot K_{53} - K_{23}}{K_{21} - jK_{51}\cot(kL_A)};\ H_3 = K_{11}H_1 + K_{12};$$

$$H_4 = K_{11}H_2 + K_{13};\ H_5 = K_{31}H_1 + K_{32};\ H_6 = K_{31}H_2 + K_{33};\ H_7 = K_{41}H_1 + K_{42};$$

$$H_8 = K_{41}H_2 + K_{43};\ H_9 = K_{61}H_1 + K_{62};\ H_{10} = K_{61}H_2 + K_{63};\ H_{11} = \frac{\rho_o c_o H_{10}}{H_7H_{10} - H_8H_9};$$

$$H_{12} = \frac{-\rho_o c_o H_8}{H_7H_{10} - H_8H_9};\ H_{13} = \frac{\rho_o c_o H_9}{H_8H_9 - H_7H_{10}};\ H_{14} = \frac{-\rho_o c_o H_7}{H_8H_9 - H_7H_{10}};$$

$$H_{15} = H_3H_{11} + H_4H_{13};\ H_{16} = H_3H_{12} + H_4H_{14};\ H_{17} = H_5H_{11} + H_6H_{13};$$

$$H_{18} = H_5H_{12} + H_6H_{14}$$